Purely Spatial Quantum Diffusion of H Atoms in Solid H_2 at Temperatures below 1 K

S. Sheludiakov, D. M. Lee, and V. V. Khmelenko*
Institute for Quantum Science and Engineering, Department of Physics and Astronomy, Texas A&M University, College Station, Texas 77843, USA

J. Järvinen, J. Ahokas, and S. Vasiliev
Department of Physics and Astronomy, University of Turku, 20014 Turku, Finland

(Received 23 December 2020; accepted 14 April 2021; published 12 May 2021)

We report on a direct measurement of the quantum diffusion of H atoms in solid molecular hydrogen films at $T = 0.7$ K. We obtained a rate of pure spatial diffusion of H atoms in the H_2 films, $D^d = 5(2) \times 10^{-17}$ cm^2 s^{-1}, which was 2 orders of magnitude faster than that obtained from H atom recombination, the quantity used in all previous work to characterize the mobility of H atoms in solid H_2. We also observed that the H-atom diffusion was significantly enhanced by injection of phonons. Our results provide the first measurement of the pure spatial diffusion rate for H atoms in solid H_2, the only solid state system beside ^{3}He – ^{4}He mixtures, where atomic diffusion does not vanish even at temperatures below 1 K.

DOI: 10.1103/PhysRevLett.126.195301

Quantum properties are best manifested for the lightest elements: helium and hydrogen. Atoms of H and ^{3}He introduced into the crystals of molecular hydrogen and helium-4, respectively, behave like a weakly interacting gas of quasiparticles, impuritons, and diffuse through the lattice by means of quantum tunneling [1–3]. Light masses and weak interactions make solid ^{3}He – ^{4}He mixtures and H_2 crystals with embedded H atoms the only solid-state systems where atomic mobility does not vanish even at temperatures below 1 K. Moreover, it manifests itself in a separation of solid ^{3}He – ^{4}He mixtures [4,5] and tunneling chemical reactions of hydrogen isotopes in solid molecular hydrogens [6–8], the lowest temperature chemical reactions observed in solids [9,10].

Atomic tunneling in regular lattices proceeds within a certain band with a width proportional to the atom zero-point energies. Such an ideal regime of quantum diffusion through identical potential wells was successfully staged and investigated for atoms in optical lattices [11–14]. Resonant tunneling in real solids, however, becomes disrupted due to lattice irregularities. As a result, diffusion slows down dramatically when the tunneling state mismatch due to lattice imperfections becomes comparable to the tunneling bandwidth [15,16]. Phonons can compensate for the tunneling state mismatch and promote tunneling motion of the impurities. Diffusion of ^{3}He atoms in solid ^{4}He studied by the NMR spin-echo technique indeed revealed a clear dependence of the diffusion rate on impurity concentration and temperature [17,18].

The situation for the lightest element, atomic hydrogen, embedded in solid H_2 is even more exotic. Unlike a simple exchange of positions taking place in solid heliums, H atoms in solid H_2 diffuse at $T < 1$ K by a different mechanism, through a repetition of the most elementary chemical reaction, $H + H_2 = H_2 + H$ [19]. Hydrogen atoms are unstable and tend to recombine when they occupy adjacent lattice sites, resulting in formation of H_2 molecules in high vibration levels ($E_{H_2} \sim 4.48$ eV). The relaxation process of vibrational energy is rather slow and accompanied by phonon emission. The H atom diffusion rate is, therefore, conventionally measured through a decrease of the H atom concentration due to their recombination. Similar to the diffusion of ^{3}He atoms in solid ^{4}He, the rate of the $H + H_2 = H_2 + H$ tunneling reaction in solid H_2 slows down dramatically when H atoms distort the periodic matrix potential upon approaching each other [20] and leading to the energy level mismatch of order of tens of kelvins. Recombination of H atoms is significantly suppressed at temperatures below 0.3 K when fewer phonons are available to stimulate the H atom diffusion [21]. As a result, the recombination measurements do not provide information on a pure spatial diffusion of H atoms, when the hydrogen atoms move far away from each other and do not perturb the tunneling motion of other H atoms.

The first attempts to investigate H-atom spatial diffusion were carried out by Constable *et al.* [22] who studied H atoms in macroscopically thick H_2 films by X-band electron spin resonance (ESR) at $T = 4.2$ K. However, the authors could not make a quantitative estimate of the H atom diffusion rate due to experimental uncertainties. The subsequent attempts to measure the pure spatial diffusion rates of H atoms in solid H_2 at $1.3 < T < 4.2$ K indirectly relied on H-atom catalyzed ortho-para conversion [23–25] and diffusion-limited chemical reactions of H atoms with simple organic and inorganic molecules trapped in solid H_2

[26,27]. They provided important evidence for tunneling motion of H atoms in solid H_2 and the influence of lattice defects on H atom localization but did not provide any information on the pure spatial H atom diffusion.

In the present work, we report the first observation and quantitative analysis of pure spatial H atom diffusion in solid H_2. H atoms in solid H_2 films were studied by 128 GHz ESR at temperature 0.7 K. By studying kinetics of H atom accumulation in solid H_2 films, we determined both the rates of pure H atom spatial diffusion into the H_2 film bulk and the diffusion rate estimated from the H atom recombination. We observed that the pure spatial diffusion of H atoms in solid H_2 at $T = 0.7$ K when their concentration equal to $n \sim 10^{19}$ cm^{-3} (~390 ppm) proceeds 2 orders of magnitude faster than that obtained from the H atom recombination measurements.

The experimental setup is based on an Oxford 200 dilution refrigerator which accommodates a sample cell (SC) [28,29] and a cryogenic 128 GHz ESR spectrometer [30]. The SC is attached to the refrigerator mixing chamber and also located in the center of a 4.6 T superconducting magnet. The upper semispherical mirror of the ESR Fabry-Perot resonator is made of silver-plated copper and the bottom flat mirror is a 1 cm^2 400 nm thick gold layer deposited onto a quartz crystal. This gold layer also serves as a top electrode of a quartz microbalance (QM). This arrangement makes it possible to retrieve the ESR signals of H atoms in solid H_2 and measure the H_2 film thickness during the deposition by means of the QM [31]. The auxiliary rf resonator placed near the QM was used to run a rf discharge in a helium vapor to create H atoms in solid H_2 films.

A special chamber, the dissociator [28], where we condensed hydrogen gas prior to H_2 film deposition, is anchored to the continuous heat exchanger of the dilution refrigerator. By running the rf discharge in the dissociator, we could create a steady flux of gas-phase hydrogen atoms into the SC. We used the two ESR lines of H atoms in the gas phase to calibrate our ESR signals of H atoms in solid H_2 and find an absolute number of H atoms accumulated in the molecular hydrogen films. The calibration principle is based on finding a correspondence between heat released during recombination of H atoms in the gas phase and the decrease of their ESR lines [32,33]. In this work, we also analyzed the concentration-dependent broadening and shift of the ESR lines of H atoms in solid H_2 from the ESR lines of H atoms in the gas phase in order to evaluate the local concentrations of H atoms embedded in the molecular hydrogen films [32].

We studied three as-deposited crystalline solid H_2 films: two 2.5 μm and one 0.65 μm thick (samples 1, 2, and 3, respectively). Although the samples were made of hydrogen gas with normal ortho-para content (25% para, 75% ortho), fast ortho-para conversion on the time scale of experiments ensures high para-H_2 concentration. The H_2 films were deposited either directly from a room temperature reservoir (sample 1) or by recondensing H_2 from the dissociator (samples 2 and 3) at a rate 2–3 nm/s while the sample cell was stabilized at $T = 1$ K. After that, we cooled the SC to $T = 0.7$ K and admitted a small, of order 1 μmol, amount of He gas needed to start the rf discharge in the SC. Further on, we continued to run the discharge and monitor the evolution of H atom ESR lines. Samples 1, 2, and 3 were exposed to the discharge for sixteen, eight, and fourteen days, respectively.

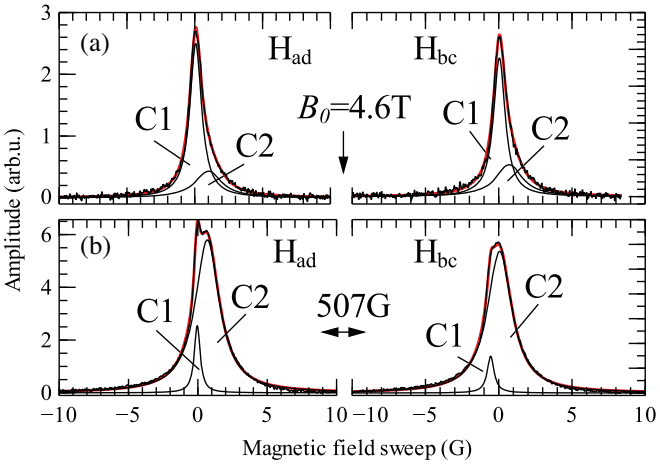

FIG. 1. ESR spectra of H atoms in the sample 1. (a) At the beginning of sample accumulation (day 2). (b) At the end of sample accumulation (day 16). See the text for further details. The relative scales are shown on the vertical axes.

The ESR lines of H atoms, H_{ad} and H_{bc}, in all three samples right after starting the discharge had a Gaussian shape which evolved to a pure Lorentzian shape after the first day of storage and rapid conversion of ortho-H_2 molecules catalyzed by H atoms. In addition to the narrow component ($C1$ in Fig. 1), a broad component [$C2$ in Fig. 1(a)] appeared in all three samples and continued to grow when time progressed. H atoms corresponding to both components had the same spectroscopic parameters, the electronic g factor, g_e, and hyperfine constant, A, which corresponded to trapping of H atoms in the substitutional sites of the H_2 lattice [32]. The two ESR line components appear shifted due to different local concentrations of H atoms corresponding to each component.

The experiments showed that accumulation of H atoms in the solid H_2 film during the rf discharge proceeds in two distinct stages. During the first stage, the local H atom concentration in the film as determined from the ESR linewidth grew rapidly and linearly with time and remained proportional to the absolute number of H atoms calculated after calibrating our ESR spectrometer (see Fig. 2). After about three days of running the discharge, the growth rate of the H atom number slowed down and showed a clear deviation from the linear increase.

Both the absolute number of H atoms and their local concentration in the samples we studied evolved identically with time as demonstrated in Figs. 2(a) and 2(b),

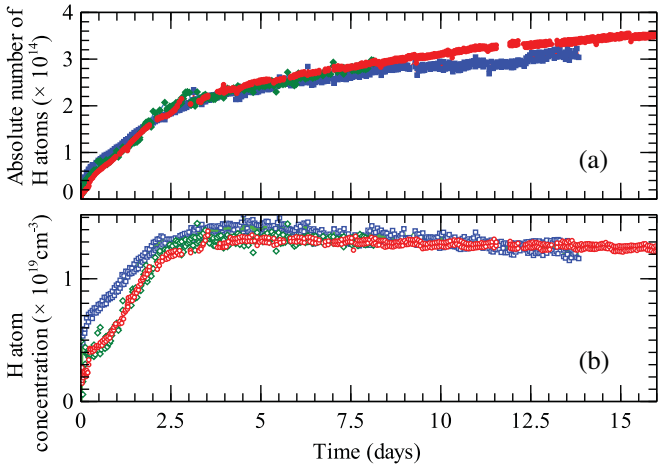

FIG. 2. (a) Time evolution of the absolute number of H atoms in samples 1, 2, and 3 (filled red circles, green diamonds, and blue squares, respectively). (b) Time evolution of the average local concentrations of H atoms in samples 1, 2, and 3 (open red circles, green diamonds, and blue squares, respectively).

respectively. Thus, for the further analysis we present only the time evolution of the number of H atoms and their local concentrations corresponding to ESR line components in sample 1 [Figs. 3(a) and 3(b), respectively]. After about 1.5 days of running the discharge, the number of H atoms corresponding to the narrower $C1$ component stopped growing and only the number of atoms corresponding to the broad component continued to increase [see Fig. 3(a)]. The local concentration of H atoms corresponding to component $C1$, however, after reaching the maximum, $n \simeq 5 \times 10^{18}$ cm^{-3} (195 ppm), became smaller in the course of the rf discharge, while that of H atom corresponding to the broad component $C2$ after reaching the value $n = 1.5 \times 10^{19}$ cm^{-3} (580 ppm) almost did not change [Fig. 3(b)].

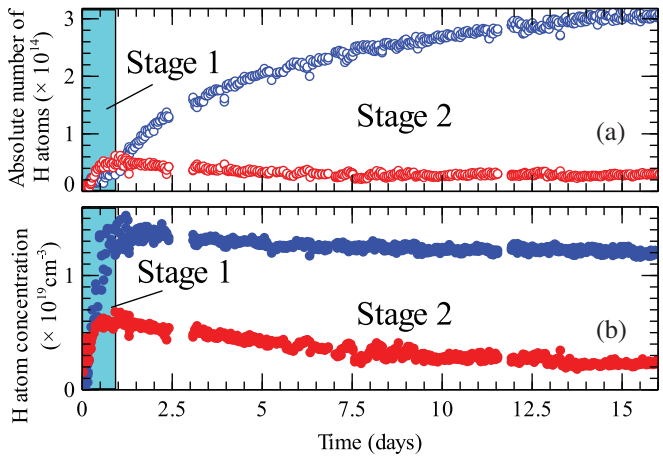

FIG. 3. Time evolution of the absolute number of H atoms (a) and concentrations (b) corresponding to $C1$ and $C2$ components in the 2.5 μm thick sample 1 shown by red and blue circles, respectively.

Similar to our previous work [37], the composite structure of the ESR lines of H atoms in solid H_2 films could be assigned to the formation of two regions in the H_2 film with low and high local H atom concentrations. The observed time dependencies of the absolute number of atoms and local concentrations of H atoms can be explained by considering formation of a layer with a high concentration of H atoms close to the H_2 film surface and followed by diffusion of the H atoms deeper into the film due to the gradient of H atom concentration. The broad component $C2$ of the H atom ESR lines corresponds to the atoms in the layer with a high local H atom concentration and the narrow $C1$ component corresponds to the averaged signal of H atoms in the film beyond this layer (see inset in Fig. 4). The H atom concentration remains uniform within this H-atom rich layer and the H atom diffusion can be considered as a propagation of the high-concentration region front deeper into the H_2 film (inset in Fig. 4).

The buildup of H atom concentration, n, in a solid H_2 film can be described by a differential equation,

$$dn/dt = k - 2k_r^d n^2 - D^d d^2 n/dx^2, \quad (1)$$

where k is the accumulation rate of H atoms due to running the discharge, k_r^d and D^d are the temperature dependent recombination rate constant and the rate of H-atom diffusion into the film bulk during the discharge, respectively, and x is the thickness of the H-atom rich H_2 layer.

At the beginning of H atom accumulation when their concentrations were low, the recombination and diffusion terms are small and the first linear term corresponding to direct dissociation of H_2 molecules in the film by electron impact dominates. In the course of continuing the discharge,

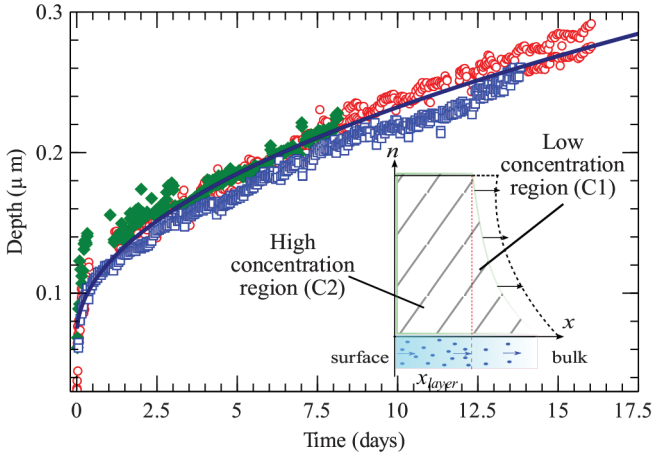

FIG. 4. Evolution of the H-atom rich layer in samples 1, 2, and 3 (open red circles, filled green diamonds, and open blue squares) while running the discharge in the sample cell. The solid black line shows a fit to the experimental data using Eq. (2) at the second stage of H atom accumulation. The inset shows the propagation of the layer with a high concentration of H atoms deeper into the bulk due to spatial diffusion.

the accumulation term eventually becomes compensated by the H-atom recombination which leads to saturation of the H atom local concentration. In the absence of H atom diffusion, evolution of the H atom concentration in time follows the $n(t) = n_{\mathrm{eq}} \tanh(-t/\tau)$ dependence and finally reaches an equilibrium concentration $n_{\mathrm{eq}} = \sqrt{k/2k_r^d}$ with a characteristic time $\tau = 1/\sqrt{2kk_r^d}$ [38]. This was indeed observed in the course of this measurement at the end of the first accumulation stage [see Fig. 3(b)]. Therefore, the first stage corresponds to a direct dissociation of H_2 molecules under the free surface of the film within a $\simeq$100 nm layer by electrons created during the rf discharge and formation of the layer with a high concentration of H atoms. From the analysis of the first accumulation stage we obtained the H-atom recombination rate, k_r^d, and the diffusion rate associated with H atom recombination, $D_r^d = k_r^d/4\pi a_0$, where $a_0 = 3.79$ Å is the solid H_2 lattice constant. The values obtained are $k_r^d = 2(1) \times 10^{-25}$ cm^3 s^{-1} and $D_r^d = 4(2) \times 10^{-19}$ cm^2 s^{-1}.

At the second stage, the absolute number of H atoms in the samples continued to increase while the H atom local concentration remained constant. This provides evidence that the spatial H atom diffusion prevents ESR signal saturation and is responsible for the observed H atom number increase. For the analysis of the H atom diffusion rate at the second stage, we can assume a case of 1D diffusion of H atoms into the H_2 film bulk with no radial gradient of H atom concentration in the film during the discharge being produced. We did not observe a $C2$ component narrowing expected from the Fick's second law diffusion term $D^d d^2n/dx^2$ as more and more H atoms diffused deeper into the film. Therefore, we suggest that no H atom concentration gradient is formed in the H_2 film layer rich in H atoms corresponding to component $C2$. Unlike the recombination term, the latter term describes the pure spatial H atom diffusion which does not lead to H atom recombination. We calculated the thickness of the H-atom rich layer, x in Eq. (1), as a function of time based on the absolute number of H atoms determined from the calibrated ESR line integrals, the local concentrations estimated from the H atom ESR linewidths, and the known flat mirror surface area (see Fig. 4). The distance the front of the layer rich in H propagates deeper into the film bulk is defined by the solution of Fick's second law as

$$x = \sqrt{6D^d t}. \tag{2}$$

We obtained the value $D^d = 5(2) \times 10^{-17}$ cm^2 s^{-1} by fitting the data presented in Fig. 4. The pure spatial diffusion rate is 2 orders of magnitude larger than that calculated from the H atom recombination rate constant, D_r^d, measured at the same temperature, $T = 0.7$ K, and the ongoing rf discharge. This provides evidence that the spatial diffusion measured under conditions when H atoms can avoid approaching each other is considerably faster than that obtained from recombination measurements when H atoms have to approach each other in order to recombine.

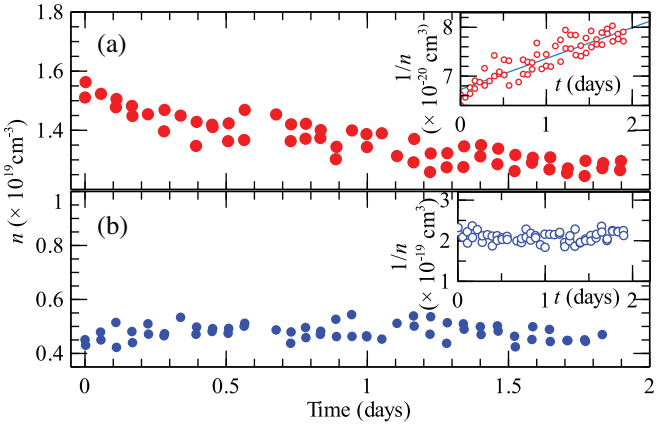

FIG. 5. (a) Time evolution of the local concentration of H atoms corresponding to the broad component $C2$ in sample 3 after stopping the discharge. Inset: inverse concentration of H atoms corresponding to component $C2$ as a function of time. (b) Time evolution of the concentration of H atoms corresponding to the narrow component $C1$. Inset: inverse concentration of H atoms corresponding to component $C1$ as a function of time.

All the experiments described above were performed while running the discharge which creates a flux of phonons in the H_2 films. In order to clarify the role of phonons created during the discharge on H atom diffusion and recombination, we additionally measured the time evolution of the H atom ESR lines in sample 3 at $T = 0.7$ K after finishing the H atom accumulation and stopping the discharge. We observed a clear decrease of the H atom concentration related to the broader component $C2$ [Fig. 5(a)]. The concentration of H atoms associated with the narrower component $C1$ did not change within the accuracy of our measurement [Fig. 5(b)].

The results of recombination studies at $T = 0.7$ K in sample 3 show that the H atom recombination and diffusion rates without the discharge, $k_r = 4(2) \times 10^{-26}$ and $D_r = 8(4) \times 10^{-20}$ cm^2 s^{-1}, are clearly smaller than those during the H atom accumulation. This emphasizes the role of phonons in overcoming the tunneling level mismatch required for the efficient quantum tunneling diffusion. The enhancement of the H atom diffusion and recombination rates upon the injection of phonons also suggests a tendency of H atoms in the H_2 films we studied to localization similar to that observed for ^{3}He atoms in solid ^{4}He [39]. Because of a weaker interparticle van-der-Waals interaction and different diffusion mechanism involved, the repetition of the chemical tunneling reaction for H atoms in solid H_2 and simple exchange of positions for ^{3}He in solid He, respectively, the tunneling motion of ^{3}He atoms in solid ^{4}He at $T = 0.7$ K, $D \simeq 10^{-8}$ cm^2 s^{-1} [39], takes place much faster as compared with that of H in solid H_2 at

the same temperatures and the same concentration of impurity atoms in the host lattice [18].

In conclusion, we carried out the first measurement of pure spatial H-atom diffusion in a solid H_2 matrix. It was found that the pure H-atom spatial diffusion which does not require H atoms to approach each other proceeds 2 orders of magnitude faster as compared with the diffusion obtained from H atom recombination measurements when the energy level mismatch impedes their tunneling motion at small distances. H atom diffusion becomes significantly enhanced upon injection of phonons which stimulate the tunneling motion of H atoms in solid H_2. These results provide the first direct measurement of the pure spatial diffusion rate of H atoms in solid H_2, the only solid-state system besides solid $^3He - ^4He$ mixtures where the atomic diffusion does not vanish at temperatures below 1 K.

This work has been supported by NSF Grant No. DMR 1707565, ONR Grant N00014-20-1-2184, and Academy of Finland Grant No. 317141.

*khmel@physics.tamu.edu

[1] A. F. Andreev and I. M. Lifshitz, Sov. Phys. JETP **29**, 1107 (1969).
[2] C. Cazorla and J. Boronat, Rev. Mod. Phys. **89**, 035003 (2017).
[3] Z. G. Cheng and J. Beamish, Phys. Rev. Lett. **121**, 225304 (2018).
[4] B. A. Fraass and R. O. Simmons, Phys. Rev. B **36**, 97 (1987).
[5] C. Huan, L. Yin, J. S. Xia, D. Candela, B. P. Cowan, and N. S. Sullivan, Phys. Rev. B **95**, 104107 (2017).
[6] H. Tsuruta, T. Miyazaki, K. Fueki, and N. Azuma, J. Phys. Chem. **87**, 5422 (1983).
[7] S. I. Kiselev, V. V. Khmelenko, and D. M. Lee, Phys. Rev. Lett. **89**, 175301 (2002).
[8] T. Kumada, J. Chem. Phys. **124**, 094504 (2006).
[9] S. Sheludiakov, J. Ahokas, J. Järvinen, D. Zvezdov, L. Lehtonen, O. Vainio, S. Vasiliev, D. M. Lee, and V. V. Khmelenko, Phys. Chem. Chem. Phys. **18**, 29600 (2016).
[10] S. Sheludiakov, J. Ahokas, J. Järvinen, L. Lehtonen, O. Vainio, S. Vasiliev, D. M. Lee, and V. V. Khmelenko, Phys. Chem. Chem. Phys. **19**, 2834 (2017).
[11] C. Sias, A. Zenesini, H. Lignier, S. Wimberger, D. Ciampini, O. Morsch, and E. Arimondo, Phys. Rev. Lett. **98**, 120403 (2007).
[12] H. Lignier, C. Sias, D. Ciampini, Y. Singh, A. Zenesini, O. Morsch, and E. Arimondo, Phys. Rev. Lett. **99**, 220403 (2007).
[13] C. Sias, H. Lignier, Y. P. Singh, A. Zenesini, D. Ciampini, O. Morsch, and E. Arimondo, Phys. Rev. Lett. **100**, 040404 (2008).
[14] A. Zenesini, C. Sias, H. Lignier, Y. Singh, D. Ciampini, O. Morsch, R. Mannella, E. Arimondo, A. Tomadin, and S. Wimberger, New J. Phys. **10**, 053038 (2008).
[15] Y. Kagan and L. A. Maksimov, Sov. Phys. JETP **57**, 459 (1983).
[16] Y. Kagan, J. Low Temp. Phys. **87**, 525 (1992).
[17] A. Widom and M. G. Richards, Phys. Rev. A **6**, 1196 (1972).
[18] V. N. Grigoŕev, Low Temp. Phys. **23**, 3 (1997).
[19] T. Kumada, Phys. Rev. B **68**, 052301 (2003).
[20] T. Kumada, M. Sakakibara, T. Nagasaka, H. Fukuta, J. Kumagai, and T. Miyazaki, J. Chem. Phys. **116**, 1109 (2002).
[21] J. Ahokas, J. Järvinen, V. V. Khmelenko, D. M. Lee, and S. Vasiliev, Phys. Rev. Lett. **97**, 095301 (2006).
[22] J. H. Constable, J. R. Gaines, P. E. Sokol, and P. C. Souers, J. Low Temp. Phys. **58**, 467 (1985).
[23] V. Shevtsov, A. Frolov, I. Lukashevich, E. Ylinen, P. Malmi, and M. Punkkinen, J. Low Temp. Phys. **95**, 815 (1994).
[24] T. Kumada, S. Mori, T. Nagasaka, J. Kumagai, and T. Miyazaki, J. Low Temp. Phys. **122**, 265 (2001).
[25] A. I. Strom, K. L. Fillmore, and D. T. Anderson, Low Temp. Phys. **45**, 676 (2019).
[26] L. O. Paulson, F. M. Mutunga, S. E. Follett, and D. T. Anderson, J. Phys. Chem. A **118**, 7640 (2014).
[27] M. E. Balabanoff, M. Ruzi, and D. T. Anderson, Phys. Chem. Chem. Phys. **20**, 422 (2018).
[28] See Fig. 1 of the article's Supplemental Material for a sample cell schematic.
[29] S. Sheludiakov, D. M. Lee, V. V. Khmelenko, J. Järvinen, J. Ahokas, and S. Vasiliev, Rev. Sci. Instrum. **91**, 063901 (2020).
[30] S. Vasilyev, J. Järvinen, E. Tjukanoff, A. Kharitonov, and S. Jaakkola, Rev. Sci. Instrum. **75**, 94 (2004).
[31] S. Sheludiakov, J. Ahokas, O. Vainio, J. Järvinen, D. Zvezdov, S. Vasiliev, V. V. Khmelenko, S. Mao, and D. M. Lee, Rev. Sci. Instrum. **85**, 053902 (2014).
[32] J. Ahokas, O. Vainio, S. Novotny, J. Järvinen, V. V. Khmelenko, D. M. Lee, and S. Vasiliev, Phys. Rev. B **81**, 104516 (2010).
[33] See Supplemental Material at http://link.aps.org/supplemental/10.1103/PhysRevLett.126.195301 for a discussion of the spectrometer calibration which includes Refs. [34–36].
[34] J. Järvinen, J. Ahokas, and S. Vasiliev, J. Low Temp. Phys. **147**, 579 (2007).
[35] J. Ahokas, O. Vainio, J. Järvinen, V. V. Khmelenko, D. M. Lee, and S. Vasiliev, Phys. Rev. B **79**, 220505(R) (2009).
[36] C. Poole, *Electron Spin Resonance: A Comprehensive Treatise on Experimental Techniques*, Dover books on physics (Dover Publications, New York, 1996).
[37] J. Järvinen, V. V. Khmelenko, D. M. Lee, J. Ahokas, and S. Vasiliev, J. Low Temp. Phys. **162**, 96 (2011).
[38] G. W. Collins, P. C. Souers, J. L. Maienschein, E. R. Mapoles, and J. R. Gaines, Phys. Rev. B **45**, 549 (1992).
[39] V. Mikheev, V. Maidanov, and N. Mikhin, Solid State Commun. **48**, 361 (1983).